APPENDIX THREE

Introduction to Optical Waveguiding in Simple Double-Heterostructures

A3.1 INTRODUCTION

Starting from Maxwell's equations a wave equation (sometimes referred to as the Helmholtz equation), which is very analogous to Schrödinger's equation, can be derived:

$$\nabla^2 \mathscr{E} = \mu\varepsilon \frac{\partial^2 \mathscr{E}}{\partial t^2}, \tag{A3.1}$$

where ε is the dielectric constant and μ is the magnetic permeability. In this derivation it is assumed that ε is uniform in space, and both μ and ε can be complex, although for the semiconductor materials of interest, $\mu \approx \mu_0$. The imaginary part of ε, includes the gain or loss that can occur in these materials. We are searching for time-harmonic fields propagating in the z-direction, so we try

$$\mathscr{E}(x, y, z, t) = \hat{\mathbf{e}}_t E_0 U(x, y) e^{j(\omega t - \tilde{\beta} z)}, \tag{A3.2}$$

as a solution to Eq. (A3.1). The unit vector $\hat{\mathbf{e}}_t$ gives the polarization. E_0 has units of volts, $U(x, y)$ has units of per unit length, and it is usually assumed to be normalized such that $\int |U(x, y)|^2 \, dA = 1$. Plugging Eq. (A3.2) into (A3.1) and factoring out common terms, we find that the transverse amplitude function, $U(x, y)$, must satisfy

$$\nabla^2 U(x, y) + [\tilde{n}^2 k_0^2 - \tilde{\beta}^2] U(x, y) = 0, \tag{A3.3}$$

where the square of the index of refraction $\tilde{n}^2 = \varepsilon/\varepsilon_0$, the free-space propagation

constant, $k_0^2 = \omega^2 \mu_0 \varepsilon_0 = (2\pi/\lambda)^2$, and both $\tilde{n}$ and the propagation constant in the z-direction, $\tilde{\beta}$, are complex. Expanding $\tilde{\beta} = \beta + j\beta_i$, we see from the form of Eq. (A3.2) that $\beta = \omega/v_p$, where v_p is the velocity of a phase front, or the phase velocity. We can also introduce an effective index of refraction, $\bar{n}$, so that $\beta = k_0 \bar{n} = \omega \bar{n}/c = 2\pi \bar{n}/\lambda$. In Chapter 2 we model how β_i contains the gain and internal loss terms in a laser.

A3.2 THREE-LAYER SLAB DIELECTRIC WAVEGUIDE

As shown in Fig. A3.1, the double heterostructure used in diode lasers provides a three-layer slab configuration in which each layer has a different index. More generally, in lasers we may be interested in regions where the index varies both transversely and laterally. Thus, we might modify Eq. (A3.3) to give

$$\nabla^2 U(x, y) + [\tilde{n}^2(x, y) k_0^2 - \tilde{\beta}^2] U(x, y) \approx 0. \tag{A3.4}$$

However, as indicated by the $\approx$ symbol, this now only approximately satisfies Maxwell's equations, since our derivation assumed that ε (and therefore n) was uniform in space.

In the current one-dimensional slab case, we can obtain an exact solution by solving Eq. (A3.3) for uniform n in each of the three regions and then matching the boundary conditions at the interfaces. By noting that the ratio of the real to the imaginary part of the index is very large in all practical cases of interest, we can replace $\tilde{\beta}$ by β, with some assurance that the mode shape, $U(x, y)$, will not be significantly in error. We shall still use Eq. (A3.2) to include the gain or loss in the propagating mode.

The solution procedure is very similar to how we solved for the confined

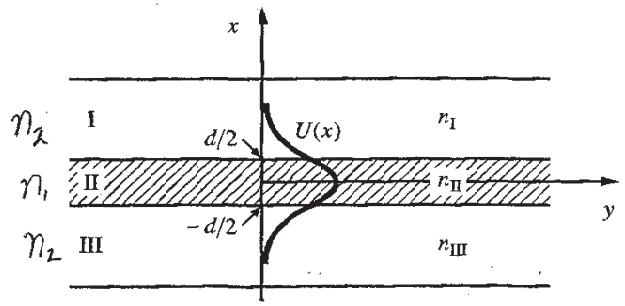

FIGURE A3.1 Schematic of a three-layer slab waveguide. Indices are assumed to be uniform in the z-direction.

states of the electron in a one-dimensional rectangular well in Appendix 1. Indeed, there is no difference in the form of the wave equation for the transverse electric field, Eq. (A3.3), and the time-independent Schrödinger's equation, Eq. (A1.5). Thus, the solutions will have the same form if the boundary conditions are analogous. As we shall see, they are analogous for the TE modes which are polarized in the y-direction, but a little different for the TM modes which are polarized in the x-direction.

A3.2.1 Symmetric Slab Case

For a symmetric three-layer slab guide ($n_{\mathrm{I}} = n_{\mathrm{III}}$), we follow the solution given in Appendix 1 for a one-dimensional potential well very closely. In the central region, we assume solutions of the form,

$$U_{\mathrm{II}}(x) = \begin{cases} A \cos k_x x \text{ (symmetric solutions)} \\ A \sin k_x x \text{ (antisymmetric solutions)} \end{cases}, \tag{A3.5}$$

In region I,

$$U_{\mathrm{I}}(x) = Be^{-\gamma x}. \tag{A3.6}$$

After substituting Eqs. (A3.5) and (A3.6) into (A3.3) with $n = n_{\mathrm{II}}$ and n_{I}, respectively, we find that

$$k_x^2 = k_0^2 n_{\mathrm{II}}^2 - \beta^2,$$

and

$$\gamma^2 = \beta^2 - k_0^2 n_{\mathrm{I}}^2. \tag{A3.7}$$

In region III, $U_{\mathrm{III}} = Be^{\gamma x}$, but by symmetry in this case ($n_{\mathrm{I}} = n_{\mathrm{III}}$), we only need to use the single boundary condition at $x = d/2$ between regions II and I.

For the TE modes at $x = d/2$, we have that $U_{\mathrm{II}} = U_{\mathrm{I}}$ and $U'_{\mathrm{II}} = U'_{\mathrm{I}}$. These conditions derive from the requirements that both the tangential electric and magnetic fields, respectively, are equal at the boundary. For the symmetric solutions, this gives

$$A \cos \frac{k_x d}{2} = Be^{-\gamma d/2}, \tag{A3.8a}$$

and

$$Ak_x \sin \frac{k_x d}{2} = B\gamma e^{-\gamma d/2}. \tag{A3.8b}$$

Dividing Eq. (A3.8b) by (A3.8a), we obtain the characteristic equation,

$$k_x \tan \frac{k_x d}{2} = \gamma. \tag{A3.9}$$

Similarly, for the antisymmetric solutions, we obtain $k_x \cot k_x d/2 = -\gamma$. Both can be included in a characteristic equation by recognizing the $\pi/2$ shift between the tan and cot functions. That is, after substituting for k_x and γ from Eqs.

(A3.7) and using $\beta = k_0 \tilde{n}$,

$$\frac{k_0 d}{2}[n_{\mathrm{II}}^2 - \tilde{n}^2]^{1/2} = \tan^{-1}\left(\frac{\tilde{n}^2 - n_{\mathrm{I}}^2}{n_{\mathrm{II}}^2 - \tilde{n}^2}\right)^{1/2} + (m-1)\frac{\pi}{2}, \tag{A3.10}$$

where $m = 1, 2, 3, \ldots$ for the fundamental and higher-order modes. For the TM modes, the continuity of the tangential electric and magntic fields at the boundaries results in an additional factor of $(n_{\mathrm{II}}^2/n_{\mathrm{I}}^2)$ on the right side of Eq. (A3.9) and inside the brackets of the $\tan^{-1}$ function in Eq. (A3.10).

The solution to this transcendental equation is done graphically as was done for confined electrons in Appendix 1 and illustrated in Fig. A1.3. As might be expected, the results are analogous for this symmetrical slab case.

A3.2.2 General Asymmetric Slab Case

To add additional generality to the present case, we can repeat the above procedures for an antisymmetric three-layer slab waveguide. That is, ($n_{\mathrm{I}} \neq n_{\mathrm{III}}$). For the TE modes, we find that the characteristic equation, Eq. (A3.9), becomes

$$\tan k_x d = \frac{(\gamma_{\mathrm{I}}/k_x) + (\gamma_{\mathrm{III}}/k_x)}{1 - \gamma_{\mathrm{I}}\gamma_{\mathrm{III}}/k_x^2}, \tag{A3.11}$$

where γ_{I} and γ_{III} are the decay constants in the upper and lower cladding regions, respectively, defined as in Eq. (A3.7). Equation (A3.11) also can be solved graphically, but it is convenient to define a normalized frequency, V, propagation parameter, b, and asymmetry parameter, a, in order to display the results. These normalized parameters are defined as follows:

$$V \equiv k_0 d(n_{\mathrm{II}}^2 - n_{\mathrm{III}}^2)^{1/2},$$

$$b \equiv \frac{\tilde{n}^2 - n_{\mathrm{III}}^2}{n_{\mathrm{II}}^2 - n_{\mathrm{III}}^2},$$

and

$$a \equiv \frac{n_{\mathrm{III}}^2 - n_{\mathrm{I}}^2}{n_{\mathrm{II}}^2 - n_{\mathrm{III}}^2}. \tag{A3.12}$$

Figure A3.2 gives plots of the normalized propagation parameter as a function of the normalized frequency for a range of normalized asymmetry parameters.

For TM modes we can use Figure A3.2 with some small error due to the neglected dielectric constant ratio that should multiply γ_{I} and γ_{III} in the dispersion relationship. The error becomes vanishingly small in weak dielectric guides.

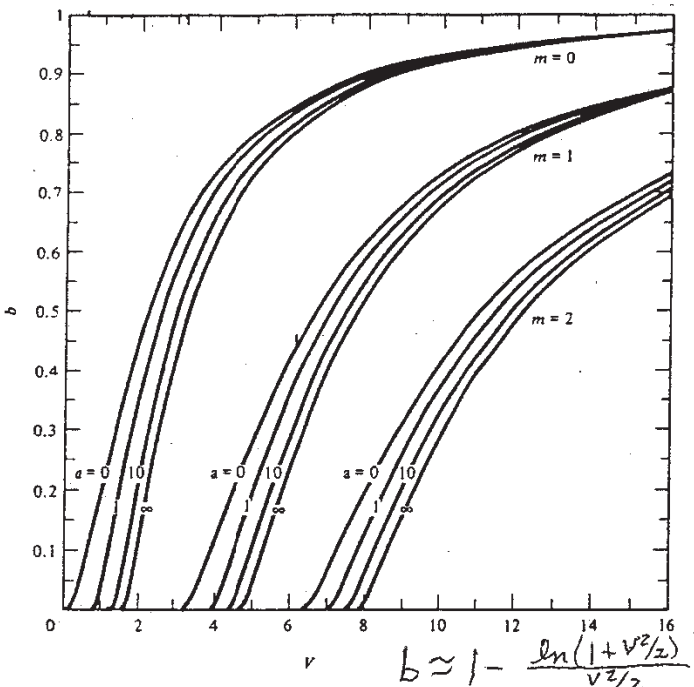

FIGURE A3.2 Normalized propagation parameter vs. normalized frequency for a range of asymmetries for the first three TE modes. After Kogelnik and Ramaswamy [1]. (Reprinted, by permission, from *Applied Optics*).

A3.2.3 Transverse Confinement Factor, Γ_x

The transverse confinement factor for the three-layer slab waveguide is defined as the fraction of the optical energy that is contained in the active slab region. As derived in Appendix 5, Eq. (A5.13), this fraction can be approximated as (neglecting $n/\bar{n}$)

$$\Gamma_x = \frac{\int_{-d/2}^{d/2} |U(x, y)|^2 \, dx}{\int_{-\infty}^{\infty} |U(x, y)|^2 \, dx}. \tag{A3.13}$$

For the symmetric case ($a = 0$), we can use Eqs. (A3.7) and (A3.5) in Eq. (A3.13)

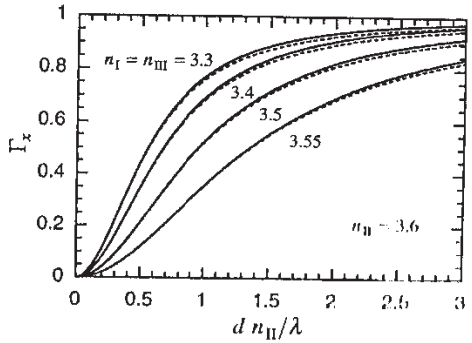

FIGURE A3.3 Comparison between the exact confinement factor (solid curve) and the approximate formula (A3.15) (dashed curve) for several values of the cladding index as a function of the guide thickness for the fundamental slab mode.

to get

$$\Gamma_x = \frac{1 + 2\gamma d/V^2}{1 + 2/\gamma d}. \tag{A3.14}$$

For the fundamental mode with relatively small index differences, Eq. (A3.14) can be approximated by

$$\Gamma_x \approx \frac{V^2}{2 + V^2}. \tag{A3.15}$$

Figure A3.3 compares the approximate formula to the exact confinement factor (neglecting $n/\bar{n}$) for several values of n_{III}.

A3.3 EFFECTIVE INDEX TECHNIQUE FOR TWO-DIMENSIONAL WAVEGUIDES

As indicated in Chapters 1 and 2, practical diode lasers usually employ waveguiding in the lateral y-direction as well as the transverse x-direction. These are referred to as either two-dimensional or channel waveguides. After Eq. (A3.4) it was suggested that exact analytic solutions to this two-dimensional problem depicted in Fig. A3.4 are impossible. The problems arise in matching the lateral boundary conditions for all values of x.

In the limiting case of very strong index discontinuities at the active–cladding interfaces, the field within the active region will fall to zero at the boundaries, and the boundary conditions can be met around the perimeter. That is, for

CHAPTER SEVEN

Dielectric Waveguides

7.1 INTRODUCTION

Thus far, we have managed to introduce quite a bit of material which made use of the transverse mode function, U, of some dielectric waveguide without knowing much about its actual form, aside from the brief introduction in Appendix 3. We have chosen this approach in part to emphasize that for many cases one does not need to know the details of all the possible transverse modes that might be supported by some dielectric layer structure. The primary reason has been to maintain a focus on the active device theme of this text and avoid distractions. In fact, we still do not intend to give an extremely detailed treatment of dielectric waveguides because that lies outside the theme of this text. Rather, we wish to introduce several different approaches to solving dielectric waveguide problems to both complement the field theory approach in Appendix 3 as well as provide the student with a broader, and perhaps more intuitive, understanding of the nature of waveguiding in these structures.

We begin by reviewing the reflection of plane waves that are incident at an arbitrary angle from a plane dielectric interface as illustrated in Fig. 7.1. The boundary conditions lead to general expressions for the reflection coefficients of both TE and TM polarizations. If the medium containing the incident plane wave has a higher index of refraction than that beyond the boundary, then we find that total internal reflection is possible. On the incident side of the dielectric boundary, the incident and reflected plane waves create a standing wave with a standing wave-ratio that becomes infinite for incident angles beyond the critical angle. Also, in this case we find that although the reflection coefficient is positive real (has a reflection phase of 0°) for incident angles smaller than the critical angle, it becomes complex beyond this angle (i.e., has a nonzero reflection phase as well as unity magnitude). Thus, for angles less than the critical angle, a standing wave maximum occurs at the boundary, but for incident angles beyond the critical angle the standing wave maximum moves back from the boundary. In what follows, we quantify the above observations.

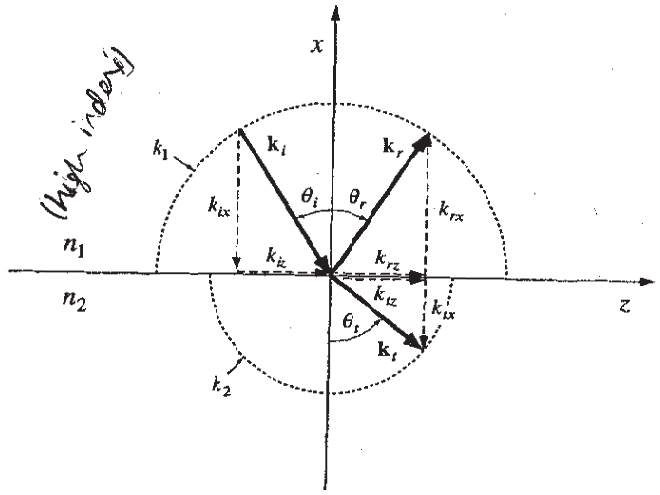

FIGURE 7.1 Illustration of a plane wave incident on a planar boundary. Angle of incidence less than critical angle.

7.2 PLANE WAVES INCIDENT ON A PLANAR DIELECTRIC BOUNDARY

Referring to the nomenclature introduced in Fig. 7.1 and earlier in Chapter 2 and Appendix 3, we express the incident, reflected, and transmitted fields for the TE and TM cases as follows:

TE

$$\begin{aligned} \mathscr{E}_i(x, z) &= \mathscr{E}_i(0, z)\hat{\mathbf{e}}_y e^{jk_{ix}x} e^{-jk_z z} \\ \mathscr{E}_r(x, z) &= \mathscr{E}_r(0, z)\hat{\mathbf{e}}_y e^{-jk_{ix}x} e^{-jk_z z} \\ \mathscr{E}_t(x, z) &= \mathscr{E}_t(0, z)\hat{\mathbf{e}}_y e^{jk_{tx}x} e^{-jk_z z} \end{aligned} \tag{7.1}$$

TM

$$\begin{aligned} \mathscr{H}_i(x, z) &= \mathscr{H}_i(0, z)\hat{\mathbf{e}}_y e^{jk_{ix}x} e^{-jk_z z} \\ \mathscr{H}_r(x, z) &= \mathscr{H}_r(0, z)\hat{\mathbf{e}}_y e^{-jk_{ix}x} e^{-jk_z z} \\ \mathscr{H}_t(x, z) &= \mathscr{H}_t(0, z)\hat{\mathbf{e}}_y e^{jk_{tx}x} e^{-jk_z z} \end{aligned} \tag{7.2}$$

Because the tangential electric fields, $\mathscr{E}$, and magnetic fields, $\mathscr{H}$, must be equal at $x = 0$, we have already used the fact that $k_{iz} = k_{rz} = k_{tz} = \beta$. Also, from this we have that $\theta_r = \theta_i$, and Snell's law, $k_i \sin\theta_i = k_t \sin\theta_t$. As always the propagation vector components are related by $k_{ix}^2 + k_{iz}^2 = k_i^2 = k_1^2 = k_0^2 n_1^2 = k_0^2 \varepsilon_1$, etc.

In any medium, the magnetic field of a plane wave is related to the electric field by Maxwell's curl equation. For the assumed forms of Eqs. (7.1) and (7.2) we have

$$\mathscr{H} = \frac{1}{\omega\mu}\mathbf{k} \times \mathscr{E}, \tag{7.3}$$

where μ is the magnetic permeability of the medium. Now, using Eqs. (7.1) and (7.2) in Eq. (7.3), and applying the boundary condition that the electric and magnetic fields are continuous at $x = 0$, we can solve for the ratio of the reflected to the incident electric fields [1, 2]. For the TE case with equal permeabilities,

$$\left.\frac{\mathscr{E}_r}{\mathscr{E}_i}\right|_{x=0} = r^{TE} = \frac{k_{tx} - k_{tx}}{k_{ix} + k_{tx}}, \tag{7.4}$$

and for the TM case,

$$\left.\frac{\mathscr{E}_r}{\mathscr{E}_i}\right|_{x=0} = r^{TM} = \frac{k_{ix} - \dfrac{\varepsilon_1}{\varepsilon_2}k_{tx}}{k_{ix} + \dfrac{\varepsilon_1}{\varepsilon_2}k_{tx}}. \tag{7.5}$$

For the case illustrated in Fig. 7.1, the index of refraction in region 1 is larger than that of region 2. Thus, as the incident angle is increased, at some point, k_{iz} equals k_2. This is called the critical angle, θ_c, defined explicitly using Snell's law by $\sin\theta_c = n_2/n_1$. For larger incident angles, k_{tx} must be imaginary to satisfy

$$k_{tx}^2 \equiv k_t^2 - k_{tz}^2 = k_t^2 - k_{iz}^2 = k_2^2 - \beta^2. \tag{7.6}$$

That is, for $k_{iz} > k_2$, $\theta_i > \theta_c$, and

$$k_{tx} = \pm j\sqrt{\beta^2 - k_2^2} = -j\gamma_{tx}, \tag{7.7}$$

where the sign of γ_{tx} is chosen for a decaying solution in region 2. This situation is shown in Fig. 7.2.

Plugging Eq. (7.7) into Eq. (7.4), we see that beyond the critical angle,

$$r^{TE} = \frac{k_{ix} + j\gamma_{tx}}{k_{ix} - j\gamma_{tx}}, \tag{7.8}$$

and

$$(\theta_i > \theta_c)$$

$$r^{TM} = \frac{k_{ix} + j\dfrac{\varepsilon_1}{\varepsilon_2}\gamma_{tx}}{k_{ix} - j\dfrac{\varepsilon_1}{\varepsilon_2}\gamma_{tx}}. \tag{7.9}$$

In both cases, we see that the magnitudes are unity, but the reflected wave

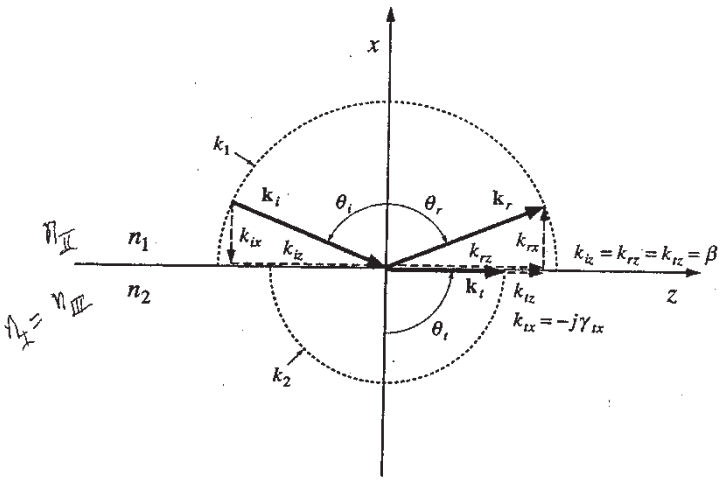

FIGURE 7.2 Plane wave incident at dielectric interface with the angle of incidence larger than the critical angle.

has a phase angle, ϕ. That is, $r = |r|e^{j\phi}$, where from Eq. (7.8) for the TE case,

$$\phi^{TE} = \tan^{-1}\left[\frac{\gamma_{tx}}{k_{ix}}\right] - \tan^{-1}\left[\frac{-\gamma_{tx}}{k_{ix}}\right], \tag{7.10}$$

or

$$\phi^{TE} = 2\tan^{-1}\left[\frac{\gamma_{tx}}{k_{ix}}\right], \tag{7.11}$$

where

$$\frac{\gamma_{tx}}{k_{ix}} = \frac{\sqrt{1 - (k_2/\beta)^2}}{\sqrt{(k_1/\beta)^2 - 1}} \quad \text{and} \quad \theta_i > \theta_c. \tag{7.12}$$

For the TM mode using Eq. (7.9) one obtains an equation analogous to Eq. (7.11) in which $\varepsilon_1/\varepsilon_2$ multiplies γ_{tx}.

As indicated in Fig. 7.3, the reflection phase angle is zero for incident angles up to the critical angle, where it begins to increase monotonically toward 180°. This results in standing waves with maxima that move away from the boundary for increasing incident angles, as also indicated. For total reflection there is still energy in region 2, but it decays exponentially away from the boundary and there is no power flow in the x-direction.

The standing waves can be calculated by summing the incident and reflected

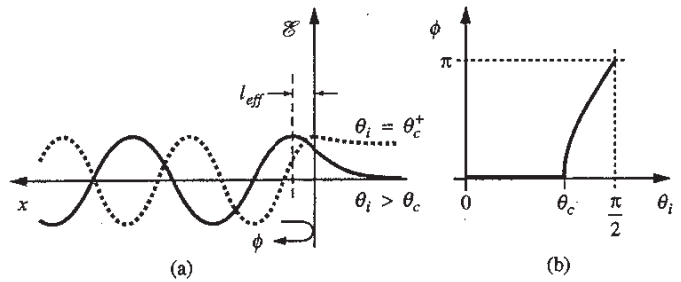

FIGURE 7.3 (a) Illustration of standing waves resulting from plane waves incident at an angle just slightly larger than (dashed) and significantly larger than (solid) the critical angle. (b) Plot of reflection phase angle vs. the angle of incidence.

waves as given by Eq. (7.1). For a TE wave with $\theta_i > \theta_c$, $\mathscr{E}_r(0, z) = \mathscr{E}_i(0, z)e^{j\phi}$. Therefore,

$$\mathscr{E}_i + \mathscr{E}_r = \mathscr{E}_i(0, z)\hat{e}_y[e^{jk_{ix}x} + e^{j\phi}e^{-jk_{ix}x}]e^{-j\beta z}, \tag{7.13}$$

or

$$\mathscr{E}_i + \mathscr{E}_r = 2\mathscr{E}_i(0, z)\hat{e}_y e^{j\phi/2}\cos(k_{ix}x - \phi/2)e^{-j\beta z}. \tag{7.14}$$

Figure 7.3 gives two examples for different ϕ, illustrating how the peak of the cosine shifts away from the interface for larger θ_i.

The separation between the maxima and the boundary in Fig. 7.3 is labeled l_{eff}, which is related to the reflection phase by

$$r = |r|e^{j\phi} = e^{-2jk_{ix}(-l_{eff})} = e^{2jk_{ix}l_{eff}},$$

or

$$2l_{eff} = \phi/k_{ix}. \tag{7.15}$$

7.3 DIELECTRIC WAVEGUIDE ANALYSIS TECHNIQUES

7.3.1 Standing Wave Technique

Now, with the above preparation, we can begin to consider the construction of a waveguide that makes use of multiple total internal reflections. In Fig. 7.4 a standing wave resulting from the total internal reflection of a plane wave (such as is shown in Fig. 7.3) is illustrated. The first maxima occurs a distance l_{eff} from the boundary as discussed above. The dashed lines correspond to symmetry planes where for the given angle of incidence another boundary identical to the original one could be inserted without changing the standing wave pattern between the two boundaries.

We can see that with this construction, we have actually formed a waveguide, which traps the plane wave at the original incident angle, forcing it to zigzag

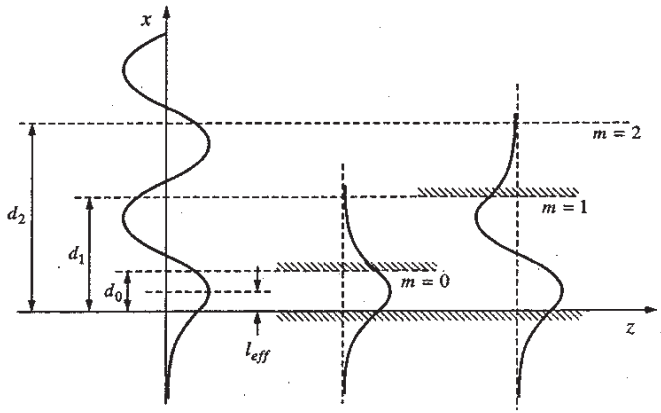

FIGURE 7.4 Construction of waveguides by inserting a second interface (top cross-hatched region) at the symmetry point on a given standing wave (i.e., given ray angle). Given standing wave at left; fundamental ($m = 0$) and first higher-order mode ($m = 1$) illustrated to the right.

indefinitely back and forth so that the net propagation of optical energy is only in the z-direction, as illustrated in Fig. 7.5. The field has the form given by Eq. (7.14) between the boundaries and is evanescent in the two outer region-2s according to $\mathscr{E}_t$ in (7.1) using (7.7) for k_{tx}.

From Fig. 7.4 the constructed waveguide width is seen to be

$$d = 2l_{eff} + m\frac{\lambda_x}{2}, \tag{7.16}$$

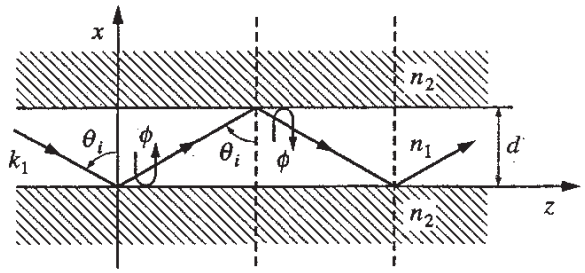

FIGURE 7.5 Illustration of zigzag ray picture of waveguiding. Each ray of the plane wave reflects off alternate boundaries with the same angle of incidence and a reflection phase that provides in-phase addition with other rays propagating in the same direction.

where m is the mode number, equal to zero for the lowest-order symmetric mode, one for the first odd mode, etc., and $\lambda_x = 2\pi/k_{ix}$ is the standing wave wavelength along the x-direction. Now, using Eqs. (7.11), (7.15), and (7.16), we obtain the waveguide dispersion relation for the TE modes,

$$d = \frac{\phi}{k_{ix}} + m\frac{\pi}{k_{ix}} = \frac{2}{k_{ix}}\tan^{-1}\left(\frac{\gamma_{tx}}{k_{ix}}\right) + m\frac{\pi}{k_{ix}}$$

or

$$k_{ix}d = 2\tan^{-1}\left(\frac{\gamma_{tx}}{k_{ix}}\right) + m\pi, \qquad m = 0, 1, 2, \ldots \tag{7.17}$$

Equation (7.17) is equivalent to Eq. (A3.10), the dispersion relationship derived in Appendix 3 for the symmetric three-layer slab waveguide. Equation (7.12) expands γ_{tx}/k_{ix} in terms of the waveguide propagation constant along z, β. For the TM modes the result is the same, except $\varepsilon_1/\varepsilon_2$ multiplies γ_{tx}.

Using these same techniques the dispersion relationship for a general three-layer asymmetric guide can be derived. As shown in Fig. 7.6 the two cladding layers have different indices of refraction. Thus, the reflection phases at the bottom and top interfaces, ϕ_2 and ϕ_3, and the separations of the standing wave maxima, l_{eff2} and l_{eff3}, respectively, are different also.

Constructing an asymmetric guide with $d = l_{eff2} + l_{eff3}$, and using

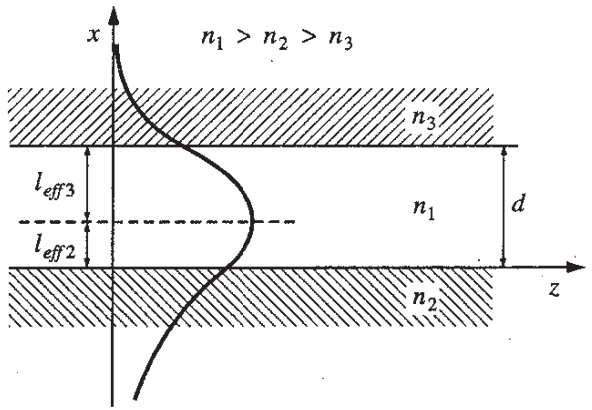

FIGURE 7.6 Fundamental mode of an asymmetric waveguide. The ray angle remains the same throughout, but the phase angle for the top reflection is larger than for the bottom. (Note the change in index definition in this chapter relative to Appendix 3.)

Eqs. (7.15) and (7.11), we find the dispersion relationship for the TE modes to be

$$k_{1x}d = \frac{\phi_2}{2} + \frac{\phi_3}{2} + m\pi = \tan^{-1}\left(\frac{\gamma_{2x}}{k_{1x}}\right) + \tan^{-1}\left(\frac{\gamma_{3x}}{k_{1x}}\right) + m\pi, \tag{7.18}$$

where as before,

$$k_{1x} = \sqrt{k_1^2 - \beta^2}, \quad \gamma_{2x} = \sqrt{\beta^2 - k_2^2}, \quad \gamma_{3x} = \sqrt{\beta^2 - k_3^2}. \tag{7.19}$$

The electric fields are given by Eq. (7.14) between the boundaries with $\phi = \phi_2$, and Eq. (7.1) in the evanescent regions using Eqs. (7.7) and (7.19) for k_{tx}.

7.3.2 Transverse Resonance

Another way of analyzing a dielectric waveguide is the transverse resonance technique. This is equivalent to the waveguide construction technique given above and the field-theory technique given in Appendix 3. As indicated in Fig. 7.7, transverse resonance means that the transverse round-trip phase must be a multiple of 2π after a complete cycle of a constituent ray. That is, the fields of an eigenmode must reproduce themselves after the plane wave components have zigzagged up and down one complete transverse cycle as the energy propagates down the guide. This is exactly the same condition as we imposed earlier in determining the modes of a Fabry–Perot resonator, only here we have generalized the situation to the case of nonnormal incidence. In other words, the component of the k-vector normal to the boundaries determines the phase progression along that direction.

For a transverse mode, we must have transverse resonance, or

$$e^{-2jk_{1x}d}e^{j\phi_2}e^{j\phi_3} = e^{-2jm\pi}, \tag{7.20}$$

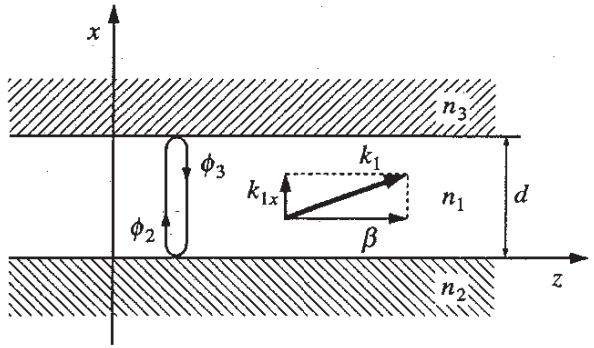

FIGURE 7.7 Waveguide cross section showing variables relevant to a transverse resonance calculation.

where the variables are as defined above in Eqs. (7.19) and (7.11). This implies that

$$2k_{1x}d - \phi_2 - \phi_3 = 2m\pi, \tag{7.21}$$

which is equivalent to Eq. (7.18).

The transverse resonance technique is a relatively simple approach to obtaining a dispersion relationship for a complex dielectric waveguiding structure. That is, regions 2 and 3 can contain a number of dielectric interfaces, and using the techniques of Chapter 3, we can calculate the net reflection coefficient from which we can obtain the reflection phases, ϕ_2 and ϕ_3. Then, Eq. (7.21) can be applied. For a lossless waveguide, the magnitude of these reflection coefficients must be unity. We shall later deal with cases where the reflection is slightly less than unity, but where the optical energy is still relatively well guided aside from a slight propagation loss.

7.3.3 Cutoff and "Leaky" or "Quasi Modes"

The point where the ray angle becomes sufficiently large (measured from the guide axis, z) so that some energy is transmitted at one boundary or the other is generally referred to as *cutoff*. (This is the point where the angle of incidence no longer exceeds the critical angle.) However, the optical energy may still continue to propagate with only modest attenuation since the reflection magnitude at the waveguide walls is still relatively large for angles near cutoff. The light that leaks out of the waveguide also tends to radiate in the forward direction so that it may run parallel to the guide for some distance. These are some of the key differences between dielectric and metal waveguides, in which cutoff tends to result in highly attenuated signals, and/or large reflections.

Put in more mathematical terms, cutoff is where $\phi_i \to 0$, or where $\beta \to k_i$, $i = 2, 3$. In other words, the waveguide propagation constant must always be larger than either of the cladding plane wave propagation constants. This situation is illustrated in Fig. 7.8 in terms of the effective index, $\bar{n} = \beta\lambda/2\pi$.

For the symmetric guide the dispersion relation, Eq. (7.17), becomes

$$k_{1x}d|_{cutoff} \leq m\pi, \qquad (n_2 = n_3) \tag{7.22}$$

from which we can see that the fundamental mode, $m = 0$, has no cutoff except at zero frequency, or zero width, d. For the asymmetric guide, the dispersion relation, Eq. (7.18), becomes

$$k_{1x}d|_{cutoff} \leq \tan^{-1}\left(\frac{\gamma_{3x}}{k_{1x}}\right) + m\pi. \qquad (n_1 > n_2 > n_3) \tag{7.23}$$

Here we see that the fundamental mode can be cutoff for some finite frequency, or a small enough waveguide width. In Appendix 3 normalized curves for the

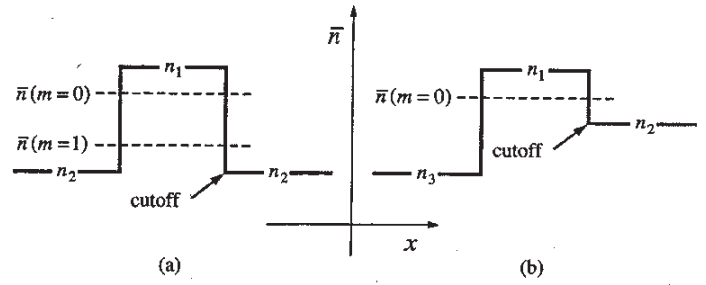

FIGURE 7.8 Illustration of effective index levels for mode numbers, m, in the (a) symmetric and (b) asymmetric cases. For decreasing frequency (increasing wavelength) $\bar{n}$ moves down toward the cutoff levels.

dispersive properties of such waveguides are given. In Fig. 7.9, we plot the effective index vs. normalized frequency for an example asymmetric guide.

Even if the reflection coefficient at one or both waveguide boundaries falls below unity for some ray angle, it is still possible to satisfy the transverse resonance condition. The dashed curves in Fig. 7.9 give the dispersion of these

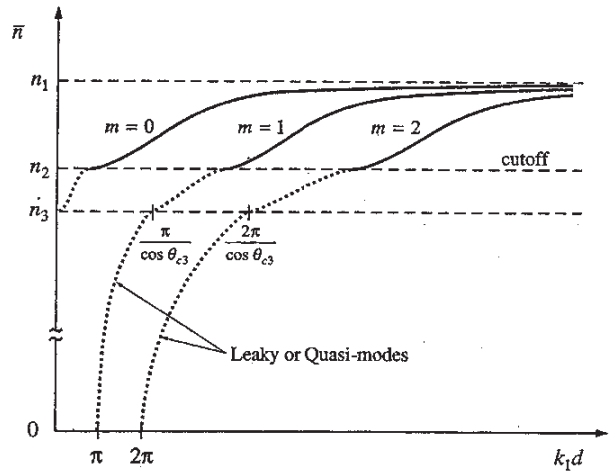

FIGURE 7.9 Schematic example of effective index dispersion curves for three lowest-order modes in an asymmetric slab. Solid curves give effective index for true guided modes. Cutoff is defined where the modes become leaky. Dotted curves indicate locus of points satisfying transverse resonance below cutoff. The angle θ_{c3} is the critical angle at the 1–3 interface. This is not the cutoff angle, which is the critical angle at the 1–2 interface.